# A computational approach for characterizing the structural basis of intrinsic coupling modes of the cerebral cortex

Arnaud Messé[1*], Lena J. Meinert[1], Karl J. Hollensteiner[2], Céline Delettre[1,3], Leigh-Anne Dell[1], Florian Pieper[2], Edgar E. Galindo-Leon[2], Benoît Larrat[4], Sébastien Mériaux[4], Jean-François Mangin[4], Isabel Reillo[5], Camino de Juan Romero[5], Víctor Borrell[5], Roberto Toro[3,6], Gerhard Engler[2], Andreas K. Engel[2], Claus C. Hilgetag[1,7]

**1** Institute of Computational Neuroscience, University Medical Center Hamburg-Eppendorf, Hamburg University, Hamburg, Germany
**2** Department of Neurophysiology and Pathophysiology, University Medical Center Hamburg-Eppendorf, Hamburg University, Hamburg, Germany
**3** Unité de Génétique Humaine et Fonctions Cognitives, Département de Neuroscience, Institut Pasteur, Paris, France
**4** NeuroSpin, CEA, Paris-Saclay University, Gif-sur-Yvette, France
**5** Developmental Neurobiology Unit, Instituto de Neurociencias, Consejo Superior de Investigaciones Científicas - Universidad Miguel Hernández, Sant Joan d'Alacant, Spain
**6** Center for Research and Interdisciplinarity, Université Paris Descartes, Paris, France
**7** Department of Health Sciences, Boston University, Boston, Massachusetts, USA

* a.messe@uke.de

## Abstract

Intrinsic coupling modes (ICMs) provide a framework for describing the interactions of ongoing brain activity at multiple spatial and temporal scales. Two types of ICMs can be distinguished, namely phase ICMs arising from phase coupling of band-limited oscillatory signals, and envelope ICMs corresponding to coupled slow fluctuations of signal envelopes. These coupling modes represent a widely used concept in modern cognitive neuroscience for probing the connectional organization of intact or damaged brains. However, the principles that shape ICMs remain elusive, in particular their relation to the underlying brain structure. Here we explored ICMs from ongoing activity of multiple cortical areas recorded from awake ferrets using chronically implanted electrocorticographic (ECoG) arrays. Additionally, we obtained different structural connectivity (SC) estimates for the regions underlying the ECoG arrays. Large-scale computational models were used to explore the ability to predict both types of ICMs. We found that simple computational models based on the SC topology already reproduce the functional coupling patterns reasonably well. Thus, the results demonstrate that patterns of cortical functional coupling as reflected in both phase and envelope ICMs are strongly related to the underlying structural connectivity of the cerebral cortex.

## Introduction

Intrinsic coupling modes reflect the patterns of functional connectivity (FC) or synchronization between neuronal ensembles during spontaneous brain activity [1].

These coupling modes represent a widely used concept in modern cognitive neuroscience for probing the connectional organization of intact or damaged brains. ICM variability has been associated with individual characteristics such as behaviour and cognitive abilities [2–5], and aberrant ICM patterns have been linked to a variety of brain diseases [6–8]. However, the principles that shape ICMs remain elusive. This concerns in particular their relation to the underlying brain structure [9]. Therefore, a careful investigation of the relation of ICMs to structural connectivity is required in order to advance our understanding of the network basis of cognition and behaviour [9–13].

Numerous studies in animals and humans have suggested that ICMs occur across a broad range of spatial and temporal scales, involving two distinct types of dynamics, namely phase ICMs (pICMs) and envelope ICMs (eICMs) [1]. Phase ICMs involve ongoing oscillatory signals with band-limited dynamics, which can be quantified by measures of phase coupling and which typically occur at frequencies between about 1 Hz and 150 Hz. By contrast, envelope ICMs correspond to coupled slow fluctuations, typically on time scales of a few seconds to minutes, which can be uncovered by the correlation of signal envelopes or signal powers. In general, ICMs can be studied with a broad variety of invasive and non-invasive methods, ranging from single-cell recordings to functional MRI. A widely used approach is the analysis of resting-state fMRI functional connectivity, based on signal correlations [14]. Using neurophysiological approaches, such as MEG, EEG, LFP or spike recordings, it becomes possible to study ICMs across a broad range of temporal and spatial scales, and in a spectrally resolved manner [11, 15–17]. The available data suggest that phase and envelope ICMs may reflect the operation of distinct coupling mechanisms [1].

The physical basis for the emergence of synchronized activity is the underlying brain structure, specifically, structural connectivity between brain regions. In this context, diffusion MRI has transformed the field by its ability to estimate the whole brain architecture of structural connections in a non-invasive manner [18]. While pioneer studies have demonstrated a tight association between the patterns of SC and fMRI-based FC [19–22], the mechanisms underlying the two types of ICMs and their relation to SC are only partly resolved. MRI-based structural connectivity remains controversial and subject to debates regarding its ability to reliably map the actual anatomical brain connectivity. On the one hand, it has been shown that tractography is susceptible to a number of biases which result in a substantial number of false positive findings [23–25]. On the other hand, tractography estimates appear fairly well correlated with tract-tracing findings [26, 27]. In any case, the impact of such biases in the context of computational modelling studies is still unknown.

Large-scale computational models have offered new mathematical tools for explicitly linking SC to ICMs [10, 28]. In particular, extensive modelling has focused on the relation of eICMs to the underlying SC. Most connectivity-based computational models presented in recent years have in fact focused on describing regional interactions at slow time scales. A variety of models have been developed for this purpose that specifically consider the influence of parameters such as structural weights, delays and noise on neural dynamics [10]. In addition, it has been shown that such slow intrinsic interactions are strongly shaped by the characteristic structural connectivity of the brain [29]. Remarkably, substantially different computational models of the local network nodes can result in similar FC patterns [30, 31]. Candidates for such similarities may include the underlying topology of brain networks as well as a potential degeneracy of the measures defining FC [32]. Much less well understood are interactions at faster time scales, that is, phase ICMs, and their relations to the underlying anatomy. Nonetheless, a few studies have reported that pICMs appear also related to SC [33, 34].

Against this background, the current study set out to pursue three hypotheses. First, we hypothesized that envelope and phase ICMs are related to SC in a complementary way depending on the frequency. Particularly, we presumed that phase ICMs are more close to SC for high frequencies, due to their temporal precision [35], while envelope ICMs should show the opposite. Second, it is generally expected that the best match to empirical ICM data can be achieved by using biologically realistic models. And finally, we expected that computational models combined with ground-truth structural connectivity data, as retrieved from retrograde tracer injections, should have more predictive power compared to when used with SC estimates from diffusion MRI tractography.

To test these hypotheses, we used data from a previous study where ongoing activity of multiple cortical areas was recorded from awake ferrets (*Mustela putorius furo*) using chronically implanted ECoG arrays [36]. The resulting recordings reflect the brain intrinsic functional network organization. Additionally, we obtained different types of SC estimates for the regions underlying the ECoG arrays [37]. Then we used large-scale computational models to explore the ability to predict both types of ICMs (Fig 1). We found that simple computational models based on the SC topology already reproduce the functional coupling patterns reasonably well. Thus, the results demonstrate that patterns of cortical functional coupling as reflected in both phase and envelope ICMs are strongly related to the underlying structural connectivity of the cerebral cortex.

# Results

Intrinsic coupling modes were extracted from ECoG data of ongoing brain activity recorded in a previous study on ferret brain dynamics [36]. The animal brain states had been objectively classified into slow-wave sleep, rapid-eye-movement sleep and awake periods, using a data-driven approach [36]. The present study focused only on data from awake periods. Phase and envelope ICMs were computed for each carrier frequency and between all pairs of electrodes using the measures of coherence and power correlation, respectively. Then electrodes were assigned to cortical areas using the atlas of Bizley et al. [38], and ICM values were averaged between these areas and across sessions and animals. Additionally, the corresponding structural connections of these areas were assembled from a variety of approaches, particularly diffusion MRI tractography [37] and retrograde tract tracing experiments in the ferret brain [39–41], as well as by homology relations with connectivity data in the cat brain. Finally, in order to predict empirical patterns of ICM, we employed two computational models of different complexity, using a biologically realistic model of a large network of spiking neurons, the SAN model [42], as well as a basic statistical model capturing the stationary behavior of a diffuse process on networks, the SAR model [43]. See Fig 1 for illustration and the Materials and Methods section for further details.

## Structure-function relationship

Contrary to our first hypothesis, phase and envelope ICMs were related to SC in a similar way, and thus independent of specific frequency bands (Fig 2). Generally, we observed a positive correlation between ICMs and SC, which increased with frequency. Also, pICMs appeared more distant to SC compared to eICMs, and the distance decreased with frequency for both ICM types.

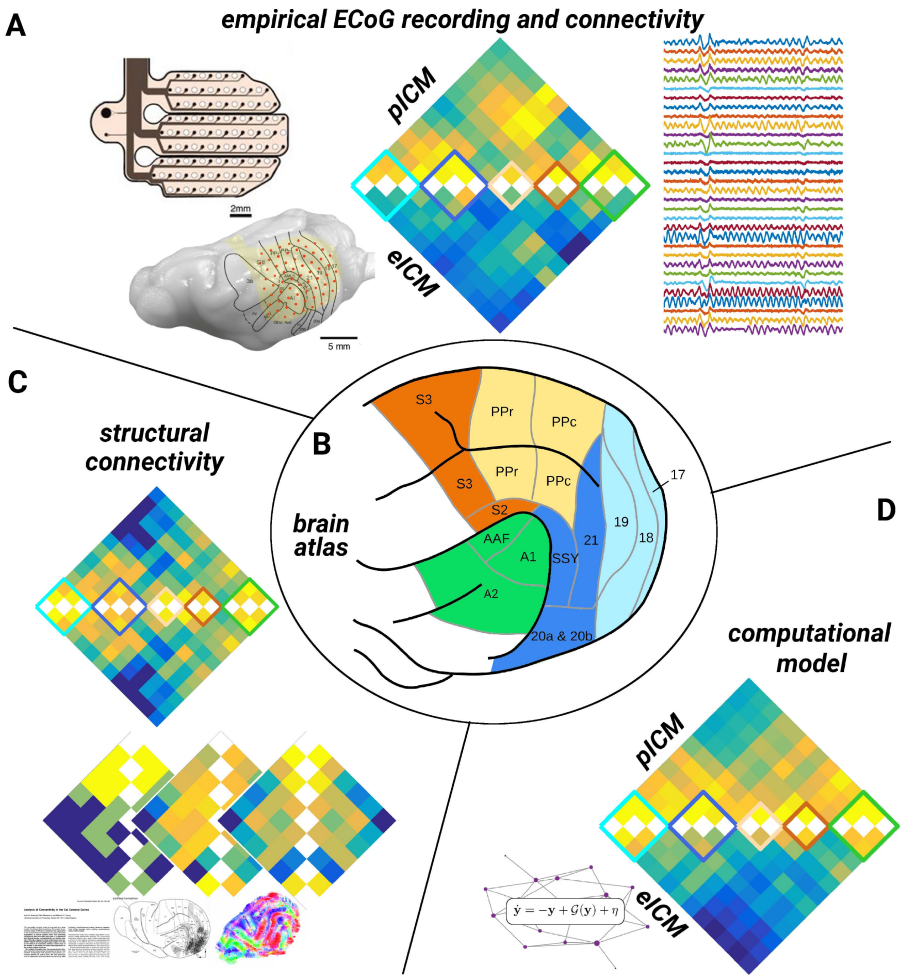


**Fig 1. Multimodal processing pipeline.** (A) Empirical ECoG recording and ICMs. Design and example of the placement over the left posterior ferret cortex. ECoG consists of 64 platinum electrodes distributed across three polymide fingers to enable the array to adapt to the curved surface of the cortex. From the resulting brain activity signals, phase and envelope ICMs were computed and mapped to the parcellation of the ferret cerebral cortex by Bizley et al. [38]. (B) Ferret cortex parcellated into 13 functionally and anatomically distinct regions according to [38]. Abbreviations: LS: lateral sulcus; SSS: suprasylvian sulcus; A: anterior; P: posterior; M: medial; L: lateral; S2/S3: somatosensory cortex 2 & 3; PPr/c: rostral/caudal posterior parietal cortex; 17,18,19,20,21: occipital/visual cortex; SSY: suprasylvian field; A1/A2: primary and secondary auditory cortex; AAF: anterior auditory field. (C) Patterns of structural connectivity from diverse anatomical sources (Cat homology, tract-tracing, and diffusion MRI tractography. (D) Large-scale computational brain models. Example of simulated phase and envelope ICMs.

## Predicting intrinsic coupling modes

We employed two computational models of different complexity: the spiking attractor network (SAN) model, a biologically realistic model of a large network of spiking neurons, and the spatial autoregressive (SAR) model, a statistical model capturing the stationary behavior of a diffuse process on networks. In general, the computational

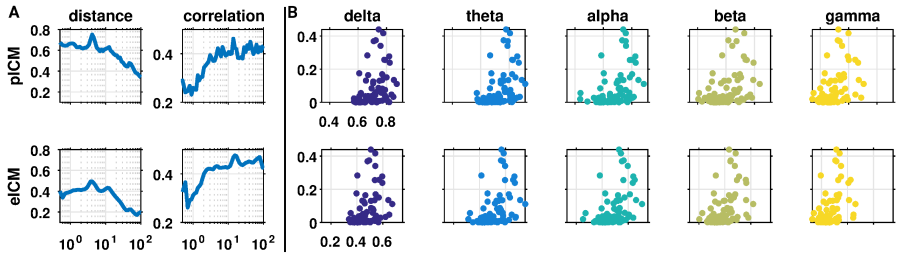


**Fig 2. Structure-function relationship.** (A) Distance and correlation of structural connectivity with phase and envelope ICMs as a function of the carrier frequency. (B) Scatter plots of ICMs versus SC across canonical frequency bands.

models predicted ICMs better than SC by itself. Contrary to our second hypothesis, the simple SAR model outperformed the predictions of empirical ICMs compared to the SAN model (Figs 3 and 4). Distance as a measure of goodness of fit appeared to be more sensitive and appropriate compared to the classic measure of correlation, because there exist no clear coupling strength values that maximized the correlation between empirical and simulated ICMs and coupling strength values with maximal correlations generally led to patterns of simulated ICMs distant from the empirical ones.

For the SAN model, the predictions appeared more nuanced depending on the measure (distance or correlation) and the frequency (Fig 3). Regarding the SAR model, we observed stable predictive values across frequencies with a significant reduction of the distance to ICMs compared to SC and only slight increases in correlation (Fig 4). Compared to the SAN model, the SAR model had a clear predictive peak depending on the coupling strength.

### Influence of the sources of structural data

While diffusion MRI tractography is the only non-invasive approach able to map whole-brain structural connectivity, one may wonder how its limitations (such as lack of directionality) and potential biases (false positives) may affect the predictive ability of connectivity-based computational models. When we compared the predictive power of the SAR model on the basis of different types of SC estimates, only very subtle differences appeared (Fig 5). All three sources of anatomical data gave rise to similar results, which is partly expected given that they are also to some extent inter-correlated. While we cannot distinguish the anatomical data in terms of distance between simulated and empirical ICMs, more pronounced differences appeared for the correlation between simulated and empirical ICMs. Here, SC based on diffusion MRI tractography and tract-tracing data had similar and higher predictive power than structural connectivity data derived by homology relations from cat connectivity.

## Discussion

In the present study, we investigated the relationship between structural connectivity and intrinsic coupling modes in the ferret brain. We also explored and compared the performance of two connectivity-based computational models of very different complexity in modelling envelope and phase ICMs. Finally, we compared the predictive performance of the models for different types of underlying SC data. Generally, we found that SC was strongly related to the ICMs and that a basic autoregressive model best matched the empirical data. Overall, our results suggest that phase and envelope ICMs during ongoing activity in awake ferrets strongly reflect

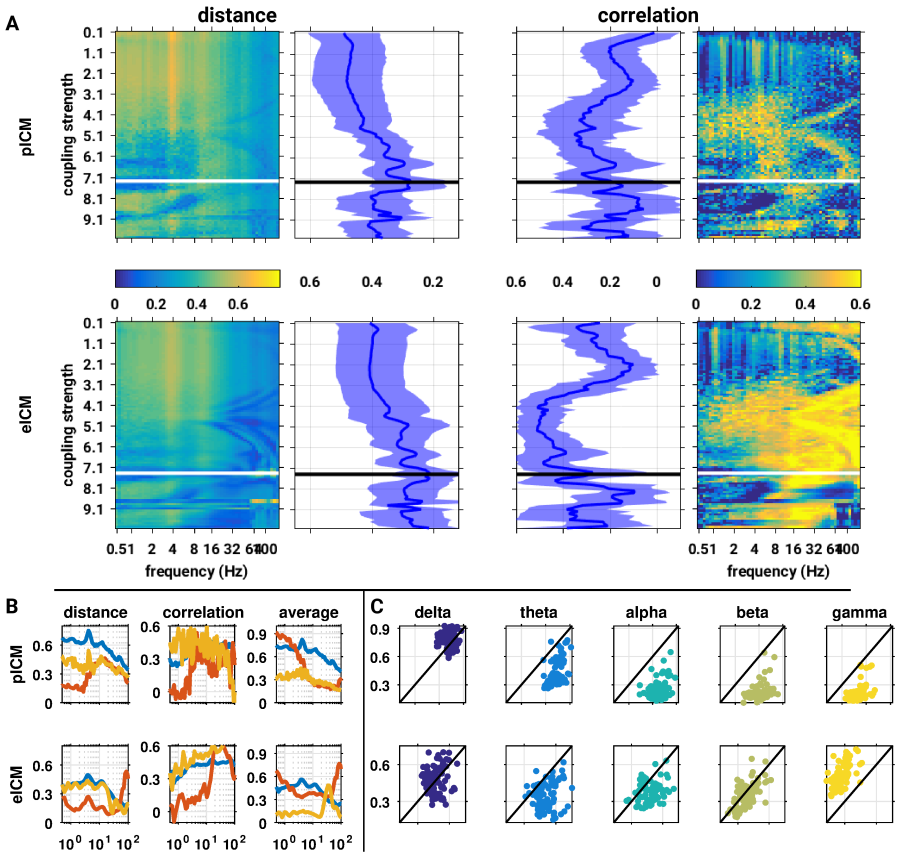


**Fig 3. Predictive power of the SAN model.** (A) Parameter space exploration. (B) Distance, correlation and averaged values of the simulated ICMs with the empirical ones as a function of the carrier frequency. Blue, red and orange curve represent the values from the structural connectivity, the simulated ICMs minimizing the distance and maximizing the correlation, respectively. (C) Scatter plots of empirical versus simulated ICMs which minimize distance, across canonical frequency bands (solid line represents the identity).

the anatomical organization of cortical networks.

In previous studies, envelope ICMs and their association with structural connectivity were mainly investigated using fMRI data, where consistent positive correlations between SC and eICMs were reported [19–22]. Some recent studies have extended and confirmed these analyses based on the refined temporal resolution offered by MEG recordings [28, 44]. The relationship between phase ICMs and structural connectivity has been explored using both EEG [33, 34, 45] and MEG [46, 47] data. Similar as for eICMs, a positive relationship between pICMs and SC has been reported consistently, but its potential frequency dependence has not yet been thoroughly investigated. Here, we confirm these observations by showing that both eICMs and pICMs are positively correlated to SC. As a matter of fact, both measures (eICMs and pICMs) appeared also correlated to each other independent of frequency. To the best of our knowledge, the present study is the first that simultaneously explored phase and envelope ICMs from the same dataset.

Using computational models of very different complexity we showed the potential of the models for predicting both types of ICMs. Surprisingly, a basic model of a diffuse stationary process appeared to best capture essential ICM patterns. The SAR

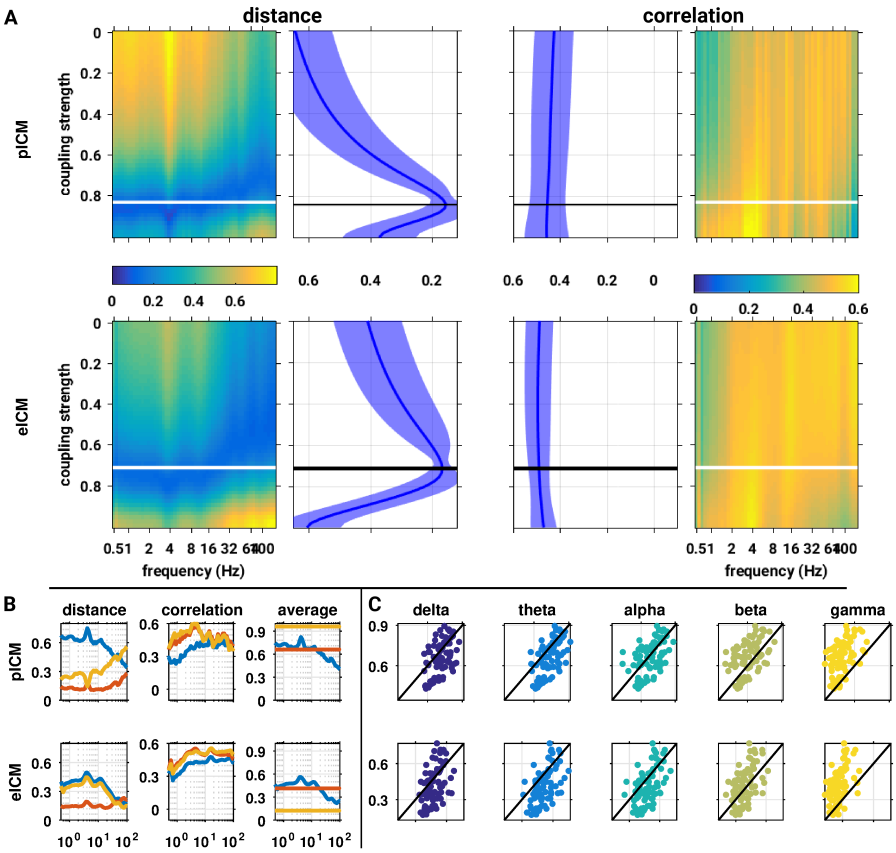


**Fig 4. Predictive power of the SAR model.** (A) Parameter space exploration. (B) Distance, correlation and averaged values of the simulated ICMs with the empirical ones as a function of the carrier frequency. Blue, red and orange curve represent the values from the structural connectivity, the simulated ICMs minimizing the distance and maximizing the correlation, respectively. (C) Scatter plots of empirical versus simulated ICMs which minimize distance, across canonical frequency bands (solid line represents the identity).

model is a generic model of diffuse process on networks and is related to the distribution of the network paths [43]. As such, and as it was previously observed in resting-state fMRI FC studies [29], patterns of functional interactions appear largely dictated by the underlying topological scaffold of the brain.

Moreover, we showed that different types of structural connectivity data provided very similar performance in terms of predicting empirical ICMs. The structural connectivity data that we used had different origins and composition (weighted undirected connectivity for diffusion MRI tractography, versus weighted directed connectivity for histological tract-tracing data, versus ordinal directed connectivity derived by homology relations from cat connectivity data). Nonetheless, they have moderate correlations between each other, which may explain their similar predictive performance.

The present results are subject to several important methodological considerations. First and foremost, despite a concept being widely adopted, brain connectivity (both structural and functional) is under massive investigations and debates on the best approaches for obtaining proper estimates and on their interpretations. While the issues related to SC have been already described above, ICM remains a concept largely

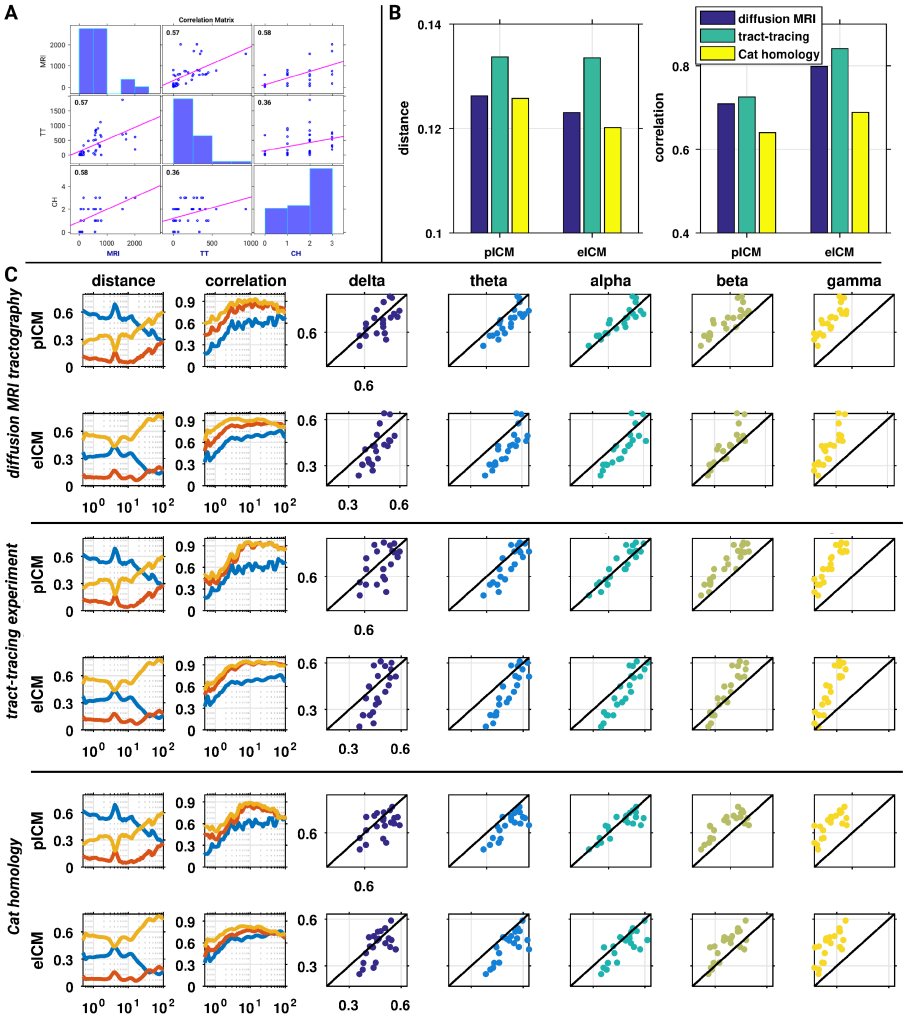


**Fig 5. Predictive power of the SAR model using different source of anatomical data.** (A) Relationship between the different types of structural connectivity. (B) Distance and correlation values of the simulated ICMs with the empirical ones as a function of the ICM and the SC data. (C) Distance and correlation values of the simulated ICMs with the empirical ones as a function of the carrier frequency. Blue, red and orange curve represent the values from the structural connectivity, the simulated ICMs minimizing the distance and maximizing the correlation, respectively. And scatter plots of empirical versus simulated ICMs which minimize distance, across canonical frequency bands (solid line represents the identity).

elusive given its vague definition and a lack of clear interpretations [32]. We here employed classic and widely used measures of coherence and power correlation as a proxy for phase and envelope ICMs, respectively. While there is an abundant literature which has provided meaningful insights into brain architecture using these measures, it would be informative to see whether alternative definitions nuance the resulting structure-function relationship. Regarding computational modelling, we make use of standard models together with their default settings (except for the coupling strength). For further refinement, it could be considered to optimize a larger number of parameters or even to incorporate knowledge from external modalities including, for

example, receptor maps [48] or microscopic anatomical (laminar) details [49].

# Materials and methods

## Intrinsic coupling modes

Intrinsic coupling modes were extracted from ECoG recordings of ongoing brain activity in awake ferrets (*Mustela putorius furo*). Data had been recorded in a previous study on five adult female ferrets [36].

### ECoG preparation and recording

To obtain the recordings from an extended set of cortical areas in freely moving animals, an ECoG array had been implanted that was co-developed with the University of Freiburg (IMTEK, Freiburg) [50]. The array covered a large portion of the posterior, parietal, and temporal surface of the left ferret brain hemisphere. Sixty-four platinum electrodes ($\varnothing$ 250 $\mu$m) were arranged equidistantly (1.5 mm) in a hexagonal manner. See Fig 1 for a schematic diagram of the ECoG layout. Ferrets had been accustomed to a recording box (45×20×52 cm), where they could move around freely while neural activity was recorded. For each animal, at least 4 separate recording sessions with a duration of more than 2 hours had been obtained. ECoG signals had been digitized at 1.4 kHz (0.1 Hz high pass and 357 Hz low pass filters), and sampled simultaneously with a 64 channel AlphaLab SnRTM recording system (Alpha Omega Engineering, Israel). A total of 23 recording sessions were analysed.

### Analysis of ECoG data

The animal brain states had been objectively classified into slow-wave sleep, rapid-eye-movement sleep and awake periods, using a data-driven approach [36]. The present study focuses only on data from awake periods.

To control for drifting and movement related artefacts the electrodes were average-referenced, the global average signal across the entire ECoG grid was subtracted from each time series. Noise epochs were detected using a threshold of 10 standard deviations. Data were rejected in a window of $\pm$ 10 s from all time points that exceeded this threshold. Then, notch filters were applied to remove line noise and its harmonics (50, 100, and 150 Hz), and the data were downsampled to 700 Hz. All data were visually inspected before further analysis to exclude ECoG or other electrical artefacts. For the present study, we analysed, on average, 34 periods of 78 s per session across animals (periods shorter than 10 s were discarded to increase statistical power).

Frequency analysis was performed on 60 logarithmically spaced frequency points from 0.1 to 160 Hz. For each session, phase and envelope ICMs were computed between all pairs of electrodes using the measures of coherence and power correlation, respectively. The coherence represents the analogue of the classic correlation for frequency resolved data. It is a normalized measure of the linear relationship between oscillatory signals, where a high value corresponds to signals with similar amplitude and aligned phases. Fast Fourier transforms were computed using a multitaper method based on Hanning windows, and phase ICMs were computed across epochs. The power correlation is a measure of the similarity between the power envelopes of the recorded signals [17, 51, 52]. Time-resolved spectra were computed by convolving the signal with a series of Morlet wavelets, and envelope ICMs were computed per frequency and averaged across epochs.

To account for inter-animal differences in the position of the ECoG-array and thus make cross-animal comparisons possible, ICM matrices were calculated at the

area-level using the atlas of Bizley et al. [38]. Each electrode was assigned to a cortical area by a 'winner-takes-all' method using its maximum overlap, and the average ICM values between these areas were computed. In total, 13 areas were covered by the ECoG-array for all animals. ICM matrices were also averaged across sessions and animals to increase statistical power. Additionally, ICMs were averaged within canonical frequency bands: 0.5-3 Hz (delta); 4-7 Hz (theta); 8-15 Hz (alpha); 16-30 Hz (beta); 30-100 Hz (gamma) for condensed representations.

All data analysis was performed using custom scripts for Matlab (Mathworks Inc) and the Fieldtrip software [53].

## Structural connectivity

Ferret brain structural connectivity data were based on diverse sources, including diffusion MRI tractography, retrograde tract tracing experiments, and from homology with connectivity data from the cat brain. The main results were based on structural connectivity estimated by diffusion MRI tractography covering the 13 areas available from the ECoG recordings. As the retrograde histological tracer experiments only investigated a restricted number of areas (7 in total, namely areas 17, 18, 19, 20, 21, PPc and PPr), the comparison of the different sources of structural connectivity were only done for that subset. Data were partly retrieved from [37].

### Diffusion MRI tractography

High resolution MRI were acquired *ex vivo* from a 2 month old ferret using a small animal 7 Tesla Bruker MRI scanner (Neurospin, Saclay, France). The ferret was euthanized by an overdose of pentobarbital and perfused transcardially with phosphate-buffered 4% paraformaldehyde. The brain was then dissected out of the skull and wrapped in wet gauze to keep it from desiccating. All procedures were approved by the IACUC of the Universidad Miguel Hernández and CSIC.

T2-weighted scan was acquired using a multi-slice multi-echo sequence with 18 echo times and 0.12 mm isotropic voxels. Diffusion MRI scan was acquired using the following parameters: TR = 40000 ms; TE = 32 ms; matrix size = 160x120x80; 0.24 mm isotropic voxels; 200 diffusion-weighted directions with b = 4000 $s/mm^2$; and 10 b = 0 at the beginning of the sequence. The total acquisition time was about 72 hours.

Diffusion MRI were first visually inspected to exclude volume with artefacts. The preprocessing steps included: local principal component analysis denoising [54], Gibbs ringing correction [55], FSL-based eddy current correction [56, 57] and B1 field inhomogeneity correction [58]. Tractography was performed based on the fiber orientation distribution estimated with a multi-tissue constrained spherical deconvolution (msmt CSD). The response functions were computed using the 'dhollander' algorithm which provides an unsupervised estimation of the white matter, grey matter and cerebrospinal fluid response functions. The msmt CSD were performed using a WM/CSF compartment model [59]. The streamline tractographies were then produced following a probabilistic algorithm (iFOD2). One million streamlines were tracked over the full brain with the parameters recommended by MRtrix3: stepsize 0.12 mm, angle 45° per voxel, minimal streamline length 1.2 mm, maximal length 2.4 cm. Structural connectivity matrices were computed using the number of streamlines connecting pairs of regions of the Bizley atlas. The matrices were inherently symmetric as diffusion MRI tractography does not provide any information about directionality.

All data analysis was performed using custom scripts for Python (Python Software Foundation) and the MRtrix3 software (`http://www.mrtrix.org/`).

### Retrograde tracer

Structural connectivity data from anatomical tract-tracing experiments on 2 years old adult ferrets were obtained from [39–41]. The experiments examined the cortico-cortical and cortico-thalamic connectivity of areas 17, 18, 19 and 21 (occipital visual cortex), 20a and 20b (temporal visual cortex), PPc and PPr (posterior parietal visual cortex) in adult ferrets by means of retrograde biotinylated dextran amine tracer. Refer to [39–41] for further details of the experimental procedures.

### Cat homology

Given similar genetic profile [60] and analogous brain structures, i.e., sulci and gyri [61, 62], it is supposed that cats (*Felis catus*) and ferrets would also share comparable connectional architectures. Thus, we used this homology to map the structural connections, which have been extensively studied in the cat [63], into the ferret. Most areas from the Bizley atlas have an homologue in the cat brain. Areas SSY corresponds to areas PMLS (posterior medial lateral suprasylvian) and VLS (ventricular lateral suprasylvian) in the cat; area PPc to area 7; area PPr to areas 5am, 5al, 5bm and 5bl; and area SIII to areas 1 and 2.

## Computational models

We employed two computational models of different complexity. The SAN model, a biologically realistic model of a large network of spiking neurons [42], and the SAR model, a basic statistical model capturing the stationary behaviour of a diffuse process on networks [43]. All models incorporated a parameter that represents the coupling strength between regions. This parameter was optimized separately for each model, see Statistics section. Structural connectivity matrices were normalized before simulations such that the matrices' rows sum to one [30, 64].

### SAN model

The SAN model is a detailed computational model based on spiking neurons and realistic synapses. A description for the microscopic level, that is within areas, is achieved by using a biologically realistic model of interconnected populations of excitatory and inhibitory neurons. The postsynaptic activity is dependent on the incoming synaptic input currents from other neurons through AMPA, NMDA and GABA receptors, as well as from external background input modelled by Poisson spike trains. Excitatory populations are interconnected at large-scale (inter-areas) *via* the structural connectivity scaled by a global coupling strength factor. For a detailed description refer to [10]

We explored coupling parameter values from 0.1 to 10 by step of 0.1. For each coupling strength value, the SAN model was simulated at a sampling frequency of 10 kHz for 5 minutes. The resulting data were then downsampled to 1 kHz. Simulated ICMs from the neuronal activity were extracted from a similar way as for the empirical data. Phase ICMs were computed by extracting epochs of 10 s.

### SAR model

The SAR model assumes that fluctuating neuronal signals ($y$) are related through a model of structural equations, which relies on expressing each signal as a linear function of the others, weighted by a global coupling strength factor $\omega$, leading to a model

$$y = \omega D y + e, \tag{1}$$

where $D$ represents the structural connectivity matrix and $e$ the input noise. According to Eq 1, $y$ is multivariate normal with covariance

$$(I - \omega D)^{-1} \sigma^2 (I - \omega D')^{-1}, \tag{2}$$

where $I$ stands for the identity matrix, $\sigma^2$ the variance of the noise, and $'$ is the regular matrix transposition.

We explored coupling parameter values from 0.001 to 0.999 by step of 0.02. The SAR model provides a closed form for the covariance matrix that can be used to directly compute the predicted ICMs *via* its normalization. Of note, the stationary SAR model does not provide frequency-resolved ICMs, but assumes a common pattern across frequencies.

### Statistics

In order to probe structure-function relationships as well as the predictive power of the different models, we computed Pearson correlations as well as distances, that is, the root-mean-square deviation, between SC, simulated and empirical ICM matrices. Diagonal elements of matrices were excluded to avoid spurious variations of the prediction. Additionally, when exploring structure-function relationships, SC was spectrally normalized (divided by its maximal eigenvalue), to avoid offsets of the distance measure due to different scales.

Coupling strength values were selected according to the predictive power measures by either maximizing the correlation or minimizing the distance between simulated and empirical ICMs. Importantly, coupling strengths were optimized separately for phase and envelope ICMs.

## Acknowledgements

This work was supported by grants from the Deutsche Forschungsgemeinschaft (DFG): SFB936/A1/A2/Z3, SPP1665/EN533/13-1 and SPP2041/HI1286/6-1/EN533/15-1. The funders had no role in study design, data collection and analysis, decision to publish, or preparation of the manuscript.

## References

1. Engel AK, Gerloff C, Hilgetag CC, Nolte G. Intrinsic coupling modes: Multiscale interactions in ongoing brain activity. Neuron. 2013;80(4):867–886. doi:10.1016/j.neuron.2013.09.038.

2. Fries P. A mechanism for cognitive dynamics: neuronal communication through neuronal coherence. Trends in Cognitive Sciences. 2005;9:474–480. doi:10.1016/j.tics.2005.08.011.

3. Fox M, Raichle ME. Spontaneous fluctuations in brain activity observed with functional magnetic resonance imaging. Nature Reviews Neuroscience. 2007;8:700–711. doi:10.1038/nrn2201.

4. Hipp JF, Engel AK, Siegel M. Oscillatory synchronization in large-scale cortical networks predicts perception. Neuron. 2011;69(2):387–396. doi:10.1016/j.neuron.2010.12.027.

5. Smith S, Nichols T, Vidaurre D, Winkler A, Behrens T, Glasser M, et al. A positive-negative mode of population covariation links brain connectivity, demographics and behavior. Nature Neuroscience. 2015;18(11):1565–1567. doi:10.1038/nn.4125.

6. Schnitzler A, Gross J. Normal and pathological oscillatory communication in the brain. Nature Reviews Neuroscience. 2005;6(4):285–296. doi:10.1038/nrn1650.

7. Uhlhaas P, Singer W. Neuronal dynamics and neuropsychiatric disorders: Toward a translational paradigm for dysfunctional large-scale networks. Neuron. 2012;75(6):963–980. doi:10.1016/j.neuron.2012.09.004.

8. Fornito A, Bullmore ET. Connectomics: A new paradigm for understanding brain disease. European Neuropsychopharmacology. 2015;25(5):733–748. doi:10.1016/j.euroneuro.2014.02.011.

9. Park HJ, Friston K. Structural and functional brain networks: From connections to cognition. Science. 2013;342(6158):1238411. doi:10.1126/science.1238411.

10. Deco G, Jirsa V, McIntosh A. Emerging concepts for the dynamical organization of resting-state activity in the brain. Nature Reviews Neuroscience. 2011;12:43–56. doi:10.1038/nrn2961.

11. Siegel M, Donner T, Engel A. Spectral fingerprints of large-scale neuronal interactions. Nature Reviews Neuroscience. 2012;13(2):121–134. doi:10.1038/nrn3137.

12. Singer W. Cortical dynamics revisited. Trends in Cognitive Sciences. 2013;17:616–626. doi:10.1016/j.tics.2013.09.006.

13. Sporns O. Contributions and challenges for network models in cognitive neuroscience. Nature Neuroscience. 2014;17(5):652–660. doi:10.1038/nn.3690.

14. Raichle M. Two views of brain function. Trends in Cognitive Sciences. 2010;14:180–190. doi:10.1016/j.tics.2010.01.008.

15. Lachaux JP, Rodriguez E, Martinerie J, Varela FJ. Measuring phase synchrony in brain signals. Human Brain Mapping;8(4):194–208. doi:10.1002/(SICI)1097-0193(1999)8:4¡194::AID-HBM4¿3.0.CO;2-C.

16. Nolte G, Bai O, Wheaton L, Mari Z, Vorbach S, Hallett M. Identifying true brain interaction from EEG data using the imaginary part of coherency. Clinical Neurophysiology. 2004;115(10):2292–2307. doi:10.1016/j.clinph.2004.04.029.

17. Hipp JF, Hawellek DJ, Corbetta M, Siegel M, Engel AK. Large-scale cortical correlation structure of spontaneous oscillatory activity. Nature Neuroscience. 2012;15:884–890. doi:10.1038/nn.3101.

18. Le Bihan D, Heidi JB. Diffusion MRI at 25: Exploring brain tissue structure and function. NeuroImage. 2011;61(2):324–341. doi:10.1016/j.neuroimage.2011.11.006.

19. Koch MA, Norris DG, Hund-Georgiadis M. An investigation of functional and anatomical connectivity using magnetic resonance imaging. NeuroImage. 2002;16(1):241–250. doi:10.1006/nimg.2001.1052.

20. Vincent JL, Patel GH, Fox MD, Snyder AZ, Baker JT, Van Essen DC, et al. Intrinsic functional architecture in the anaesthetized monkey brain. Nature. 2007;447:83–86. doi:10.1038/nature05758.

21. Hagmann P, Cammoun L, Gigandet X, Meuli R, Honey C, Wedeen V, et al. Mapping the structural core of human cerebral cortex. PLoS Biology. 2008;6:e159. doi:10.1371/journal.pbio.0060159.

22. Greicius MD, Supekar K, Menon V, Dougherty RF. Resting-state functional connectivity reflects structural connectivity in the default mode network. Cerebral Cortex. 2009;19:72–78. doi:10.1093/cercor/bhn059.

23. Thomas C, Ye F, Irfanoglu O, Modi P, Saleem K, Leopold D, et al. Anatomical accuracy of brain connections derived from diffusion MRI tractography is inherently limited. Proceedings of the National Academy of Sciences of the USA. 2014;111(46):16574–16579. doi:10.1073/pnas.1405672111.

24. Reveley C, Seth A, Pierpaoli C, Silva A, Yu D, Saunders R, et al. Superficial white matter fiber systems impede detection of long-range cortical connections in diffusion MR tractography. Proceedings of the National Academy of Sciences of the USA. 2015;112(21). doi:10.1073/pnas.1418198112.

25. Maier-Hein KH, Neher PF, Houde C, Côté MA, Garyfallidis E, Zhong J, et al. The challenge of mapping the human connectome based on diffusion tractography. Nature Communications. 2017;8(1). doi:10.1038/s41467-017-01285-x.

26. Calabrese E, Badea A, Cofer G, Qi Y, Johnson GA. A diffusion MRI tractography connectome of the mouse brain and comparison with neuronal tracer data. Cerebral Cortex. 2015;25(11):4628–4637. doi:10.1093/cercor/bhv121.

27. Donahue CJ, Sotiropoulos SN, Jbabdi S, Hernandez-Fernandez M, Behrens TE, Dyrby TB, et al. Using diffusion tractography to predict cortical connection strength and distance: A quantitative comparison with tracers in the monkey. The Journal of Neuroscience. 2016;36(25):6758–6770. doi:10.1523/JNEUROSCI.0493-16.2016.

28. Cabral J, Kringelbach ML, Deco G. Exploring the network dynamics underlying brain activity at rest. Progress in Neurobiology. 2014;114:102–131. doi:10.1016/j.pneurobio.2013.12.005.

29. Goñi J, van den Heuvel MP, Avena-Koenigsberger A, Velez de Mendizabal N, Betzel RF, Griffa A, et al. Resting-brain functional connectivity predicted by analytic measures of network communication. Proceedings of the National Academy of Sciences of the USA. 2014;111(2):833–838. doi:10.1073/pnas.1315529111.

30. Messé A, Rudrauf D, Benali H, Marrelec G. Relating structure and function in the human brain: Relative contributions of anatomy, stationary dynamics, and non-stationarities. PLoS Computational Biology. 2014;10:e1003530. doi:10.1371/journal.pcbi.1003530.

31. Messé A, Rudrauf D, Giron A, Marrelec G. Predicting functional connectivity from structural connectivity via computational models using MRI: An extensive comparison study. NeuroImage. 2015;111:65–75. doi:10.1016/j.neuroimage.2015.02.001.

32. Marrelec G, Messé A, Giron A, Rudrauf D. Functional connectivity's degenerate view of brain computation. PLoS Computational Biology. 2016;12(10):e1005031. doi:10.1371/journal.pcbi.1005031.

33. Chu C, Tanaka N, Diaz J, Edlow B, Wu O, Hämäläinen M, et al. EEG functional connectivity is partially predicted by underlying white matter connectivity. NeuroImage. 2015;108:23–33. doi:10.1016/j.neuroimage.2014.12.033.

34. Finger H, Bönstrup M, Cheng B, Messé A, Hilgetag C, Thomalla G, et al. Modeling of large-scale functional brain networks based on structural connectivity from DTI: Comparison with EEG derived phase coupling networks and evaluation of alternative methods along the modeling path. PLoS Computational Biology. 2016;12(8):e1005025. doi:10.1371/journal.pcbi.1005025.

35. Messé A, Hütt MT, König P, Hilgetag C. A closer look at the apparent correlation of structural and functional connectivity in excitable neural networks. Scientific Reports. 2015;5:7870. doi:10.1038/srep07870.

36. Stitt I, Hollensteiner KJ, Galindo-Leon E, Pieper F, Fiedler E, Stieglitz T, et al. Dynamic reconfiguration of cortical functional connectivity across brain states. Scientific Reports. 2017;7:8797. doi:10.1038/s41598-017-08050-6.

37. Delettre C, Messé A, Dell LA, Foubet O, Heuer K, Larrat B, et al. Comparison between diffusion MRI tractography and histological tract-tracing of cortico-cortical structural connectivity in the ferret brain. bioRxiv. 2019;doi:10.1101/517136.

38. Bizley JK, Nodal FR, Bajo VM, Nelken I, King AJ. Physiological and anatomical evidence for multisensory interactions in auditory cortex. Cerebral Cortex. 2007;17(9):2172–2189. doi:10.1093/cercor/bhl128.

39. Dell LA, Innocenti GM, Hilgetag CC, Manger PR. Cortical and thalamic connectivity of occipital visual cortical areas 17, 18, 19 and 21 of the domestic ferret (*Mustela putorius furo*). The Journal of Comparative Neurology. 2019;doi:10.1002/cne.24631.

40. Dell LA, Innocenti GM, Hilgetag CC, Manger PR. Cortical and thalamic connectivity of temporal visual cortical areas 20a and 20b of the domestic ferret (*Mustela putorius furo*). The Journal of Comparative Neurology. 2019;doi:10.1002/cne.24632.

41. Dell LA, Innocenti GM, Hilgetag CC, Manger PR. Cortical and thalamic connectivity of posterior parietal visual cortical areas PPc and PPr of the domestic ferret (*Mustela putorius furo*). The Journal of Comparative Neurology. 2019;doi:10.1002/cne.24630.

42. Deco G, Jirsa VK. Ongoing cortical activity at rest: Criticality, multistability, and ghost attractors. The Journal of Neuroscience. 2012;32:3366–3375. doi:10.1523/JNEUROSCI.2523-11.2012.

43. Messé A, Benali H, Marrelec G. Relating structural and functional connectivity in MRI: A simple model for a complex brain. IEEE Transactions on Medical Imaging. 2015;34:27–37. doi:10.1109/TMI.2014.2341732.

44. Garcés P, Pereda E, Hernàndez-Tamames JA, Del-Pozo F, Maestù F, Ángel Pineda-Pardo J. Multimodal description of whole brain connectivity: A comparison of resting state MEG, fMRI, and DWI. Human Brain Mapping. 2016;37(1):20–34. doi:10.1002/hbm.22995.

45. Wirsich J, Ridley B, Besson P, Jirsa V, Bénar C, Ranjeva JP, et al. Complementary contributions of concurrent EEG and fMRI connectivity for predicting structural connectivity. NeuroImage. 2017;161:251–260. doi:10.1016/j.neuroimage.2017.08.055.

46. Tewarie P, Hillebrand A, van Dellen E, Schoonheim MM, Barkhof F, Polman CH, et al. Structural degree predicts functional network connectivity: A multimodal resting-state fMRI and MEG study. NeuroImage. 2014;97:296–307. doi:10.1016/j.neuroimage.2014.04.038.

47. Meier J, Tewarie P, Hillebrand A, Douw L, van Dijk BW, Stufflebeam SM, et al. A mapping between structural and functional brain networks. Brain Connectivity. 2016;6(4):298–311. doi:10.1089/brain.2015.0408.

48. Deco G, Cruzat J, Cabral J, Knudsen GM, Carhart-Harris RL, Whybrow PC, et al. Whole-brain multimodal neuroimaging model using serotonin receptor maps explains non-linear functional effects of LSD. Current Biology. 2018;28:3065–3074. doi:10.1016/j.cub.2018.07.083.

49. Schmidt M, Bakker R, Shen K, Bezgin G, Diesmann M, van Albada SJ. A multi-scale layer-resolved spiking network model of resting-state dynamics in macaque visual cortical areas. PLoS Computational Biology. 2018;14(10):1–38. doi:10.1371/journal.pcbi.1006359.

50. Rubehn B, Bosman C, Oostenveld R, Fries P, Stieglitz T. A MEMS-based flexible multichannel ECoG-electrode array. Journal of Neural Engineering. 2009;6(3):036003. doi:10.1088/1741-2560/6/3/036003.

51. Brookes MJ, Woolrich M, Luckhoo H, Price D, Hale JR, Stephenson MC, et al. Investigating the electrophysiological basis of resting state networks using magnetoencephalography. Proceedings of the National Academy of Sciences of the USA. 2011;108:16783–16788. doi:10.1073/pnas.1112685108.

52. de Pasquale F, Della Penna S, Snyder A, Marzetti L, Pizzella V, Romani G, et al. A cortical core for dynamic integration of functional networks in the resting human brain. Neuron. 2012;74(4):753–764. doi:10.1016/j.neuron.2012.03.031.

53. Oostenveld R, Fries P, Maris E, Schoffelen JM. FieldTrip: Open source software for advanced analysis of MEG, EEG, and invasive electrophysiological data. Computational Intelligence and Neuroscience. 2011;2011:156869. doi:10.1155/2011/156869.

54. Veraart J, Novikov DS, Christiaens D, Ades-aron B, Sijbers J, Fieremans E. Denoising of diffusion MRI using random matrix theory. NeuroImage. 2016;142:394–406. doi:10.1016/j.neuroimage.2016.08.016.

55. Kellner E, Dhital B, Kiselev VG, Reisert M. Gibbs-ringing artifact removal based on local subvoxel-shifts. Magnetic Resonance in Medicine. 2016;76(5):1574–1581. doi:10.1002/mrm.26054.

56. Jenkinson M, Beckmann CF, Behrens TEJ, Woolrich MW, Smith SM. FSL. NeuroImage. 2012;62:782–790. doi:10.1016/j.neuroimage.2011.09.015.

57. Andersson JLR, Sotiropoulos SN. An integrated approach to correction for off-resonance effects and subject movement in diffusion MR imaging. NeuroImage. 2016;125:1063–1078. doi:10.1016/j.neuroimage.2015.10.019.

58. Tustison NJ, Avants BB, Cook PA, Zheng Y, Egan A, Yushkevich PA, et al. N4ITK: Improved N3 bias correction. IEEE Transactions on Medical Imaging. 2010;29(6):1310–1320. doi:10.1109/TMI.2010.2046908.

59. Jeurissen B, Tournier JD, Dhollander T, Connelly A, Sijbers J. Multi-tissue constrained spherical deconvolution for improved analysis of multi-shell diffusion MRI data. NeuroImage. 2014;103:411–426. doi:10.1016/j.neuroimage.2014.07.061.

60. Cavagna P, Menotti A, Stanyon R. Genomic homology of the domestic ferret with cats and humans. Mammalian Genome. 2000;11:886–870. doi:0.1007/s003350010172.

61. Manger PR, Nakamura H, Valentiniene S, Innocenti GM. Visual areas in the lateral temporal cortex of the ferret (*Mustela putorius*). Cerebral Cortex. 2004;14(6):676–689. doi:10.1093/cercor/bhh028.

62. Foxworthy WA, Meredith MA. An examination of somatosensory area SIII in ferret cortex. Somatosensory & Motor Research. 2011;28(1-2):1–10. doi:10.3109/08990220.2010.548465.

63. Scannell J, Blakemore C, Young M. Analysis of connectivity in the cat cerebral cortex. The Journal of Neuroscience. 1995;15(2):1463–1483. doi:10.1523/JNEUROSCI.15-02-01463.1995.

64. Cabral J, Hugues E, Sporns O, Deco G. Role of local network oscillations in resting-state functional connectivity. NeuroImage. 2011;57:130–139. doi:10.1016/j.neuroimage.2011.04.010.